14

Simulation of $Lu_2SiO_{5-z}:Y^{3+}:Ce^{3+}:Ca^{2+}$ monolithic detectors for positron emission tomography

© V.S. Tskhay, M.V. Belov, V.A. Kozlov, M.V. Zavertyaev

Lebedev Physical Institute, Russian Academy of Sciences, Moscow, Russia
E-mail: vtskhay@lebedev.ru

Received June 10, 2025
Revised July 21, 2025
Accepted July 23, 2025

We evaluate the performance of monolithic positron emission tomography (PET) detector elements depending on its scintillator crystal plate thickness (6 and 12 mm) and the surface finish (rough or polished) using a neural network to reconstruct events. A GEANT4 PET detector model was used for this study. It consisted of a LYSO crystal with a 57.6×57.6 mm face and a 64-channel Sensl ARRAYC-60035-64P-PCB photomultiplier. Separate runs were made with varying crystal parameters: thickness (6 and 12 mm) and surface finish (rough and polished), resulting in four separate event pools. A feed-forward neural network was used to reconstruct the point of 511 keV gamma interaction. The number of layers and neurons per layer were varied. The best resolution was achieved with a 6 mm thick detector with a rough finish with an average of 0.57 ± 0.01 mm for the XY plane and an average 0.89 ± 0.01 mm for the Z coordinate (depth of interaction), and a dR of 1.19 ± 0.01 mm.

Keywords: scintillating crystals, gamma radiation, positron emission tomography, neural networks.

DOI: 10.21883/0000000000

The majority of modern commercially available positron emission tomography (PET) scanners use detectors constructed from a large number of small-sized scintillation crystals ($2 \times 2 \times 20$ mm) that are assembled into units connected to multichannel silicon or multianode photomultipliers. The interaction point of a γ-quantum in such an assembly is determined by the index of a crystal in which scintillation is detected. „Monolithic" detectors are an alternative to this layout [1,2]. Crystal assemblies are substituted in monolithic detectors with large solid plates. The interaction coordinate in such a detector may be determined by examining the distribution of signals from a multichannel photomultiplier. This technique also enables the use of mathematical methods that may improve spatial resolution. One such method involves the application of artificial neural networks (ANNs). It was demonstrated that the use of ANNs provides an opportunity to reconstruct the interaction coordinate with high accuracy. In the present study, the spatial resolution of several detector versions is estimated via modeling.

A total of four detector designs were simulated. Models were constructed based on the GEANT4 software library.

A monolithic detector consists of a crystal plate connected to an array of silicon photomultipliers (Fig. 1). The model used a $64(8 \times 8)$-channel silicon photomultiplier 57.6×57.6 mm in size with its parameters corresponding to Sensl ARRAYC-60035-64P-PCB. A $Lu_2SiO_{5-z}:Y^{3+}:Ce^{3+}:Ca^{2+}$ crystal was the scintillator. The dimensions of the front face of the crystal corresponded to the photomultiplier dimensions. The crystal thickness was varied (6 and 12 mm). GEANT4 LUT Davis tables were used to parameterize the surface properties.

All the modeled detector versions had a Teflon film coating. The optical properties of the crystal were simulated based on experimental measurement data [3]. Two degrees of surface polishing were considered for each thickness: „rough" and „polished". Rough polishing was modeled with the following roughness parameters: $R_a = 0.48\,\mu$m, $R_q = 0.57\,\mu$m, and $R_{\max} = 3.12\,\mu$m. The corresponding fine polishing parameters were $R_a = 20.8$ nm, $R_q = 26.2$ nm, and $R_{\max} = 34.7$ nm. These settings are standard in GEANT4.

A layer of DOW CORNING Q2-3067 optical couplant was introduced at the crystal–photomultiplier interface.

The modeled detector assembly was irradiated with single γ-quanta with an energy of 511 keV emitted by an isotropic point source located at a distance of 35 cm from the center of the plate. Each emission of a γ-quantum by the source was considered as a single event. Events were selected if the energy of the emitted γ-quantum was released entirely in the scintillation crystal. Selected events were divided into two groups. The first group consisted of events where, prior to complete absorption, the γ-quantum was scattered at least once due to Compton interaction. These were denoted as „Compton events". In the second group of „photoelectric events", the first and only interaction was the photoelectric effect.

This subdivision is necessary, since Compton events feature several scintillation flashes at different points in the crystal, which affects the accuracy of coordinate reconstruction. In the case of photoelectric events, the flash is confined to a single point.

The number of useful events accumulated for each detector version was 2,200,000 (8,800,000 in total). Half

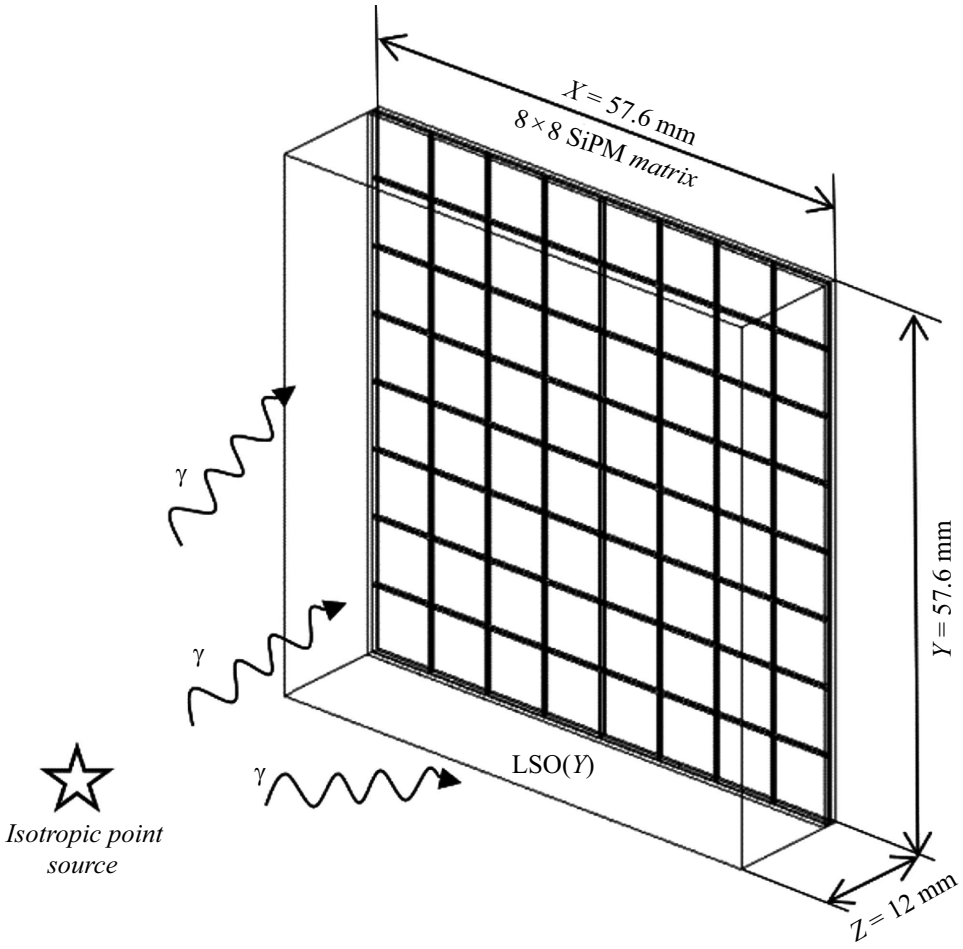

Figure 1. Detector diagram.

of them were Compton events, and the other half were photoelectric events.

In addition, 2 200 000 events were accumulated using a square source 57.6 × 57.6 mm in size located opposite the scintillator plate and emitting γ-quanta perpendicular to the face of the scintillation crystal. These data were accumulated in order to investigate possible effects that may arise when collimated sources are used in ANN training. This comparison is important, since most studies involving modeling of monolithic PET detectors use collimated sources, while real-life PET sources are always isotropic. The variation of incidence angles of γ-quanta will affect the distribution of flashes in the case of multiple Compton scattering, which, in turn, will affect the ANN training process and the accuracy of reconstruction of the interaction coordinates.

A simple feed-forward ANN [4] written in C++ was used to reconstruct the interaction point. The network contained 64 input neurons corresponding to the silicon photomultiplier channels and three output neurons corresponding to coordinates X, Y, and Z. The number of intermediate (hidden) layers varied from 1 to 3. The number of neurons in the layers did also vary between 256, 512, and 1024. A total of nine versions of the network were tested. The LReLU (leaky rectifying linear unit) activation function was used. The diagram of the neural network is shown in Fig. 2.

The ANN was trained using the backpropagation algorithm with gradient descent. Normalized sets of signals from photomultiplier cells were used as input data. The coordinates of interaction of a γ-quantum served as the output values of the network (in the case of Compton interaction, the coordinates of the first interaction were used). In each data set, 1 000 000 events with the

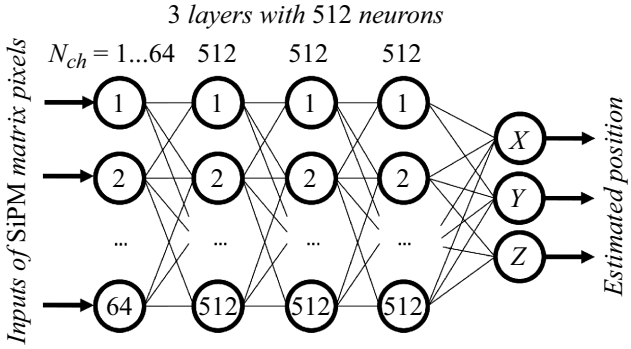

Figure 2. Structure of the artificial neural network.

Table 1. Resolution obtained using different ANN versions in different detector designs

Layers	256 neurons			512 neurons			1024 neurons		
	ΔX, mm	ΔZ, mm	ΔR, mm	ΔX, mm	ΔZ, mm	ΔR, mm	ΔX, mm	ΔZ, mm	ΔR, mm
Polished plate 6 mm in thickness									
One layer	0.62	1.34	1.59	0.57	1.27	1.5	0.55	1.16	1.4
Two layers	0.59	1.11	1.39	0.55	1.04	1.3	0.55	0.99	1.25
Three layers	0.58	1.1	1.38	0.56	1.06	1.32	0.54	1.14	1.38
Rough plate 6 mm in thickness									
One layer	0.63	1.04	1.38	0.61	0.99	1.32	0.61	0.97	1.3
Two layers	0.59	0.95	1.27	0.58	0.91	1.22	0.57	0.89	1.19
Three layers	0.59	0.96	1.27	0.55	0.92	1.2	0.58	0.96	1.26
Polished plate 12 mm in thickness									
One layer	0.86	1.16	1.69	0.8	1.1	1.59	0.86	1.11	1.65
Two layers	0.92	1.07	1.67	0.89	1.01	1.62	0.89	1.01	1.61
Three layers	0.93	1.04	1.68	0.91	1.02	1.65	0.91	1.0	1.62
Rough plate 12 mm in thickness									
One layer	0.89	1.16	1.72	0.93	1.13	1.72	0.92	1.13	1.71
Two layers	0.99	1.14	1.8	0.95	1.12	1.76	0.96	1.07	1.7
Three layers	0.98	1.1	1.77	0.97	1.08	1.73	0.93	1.09	1.72

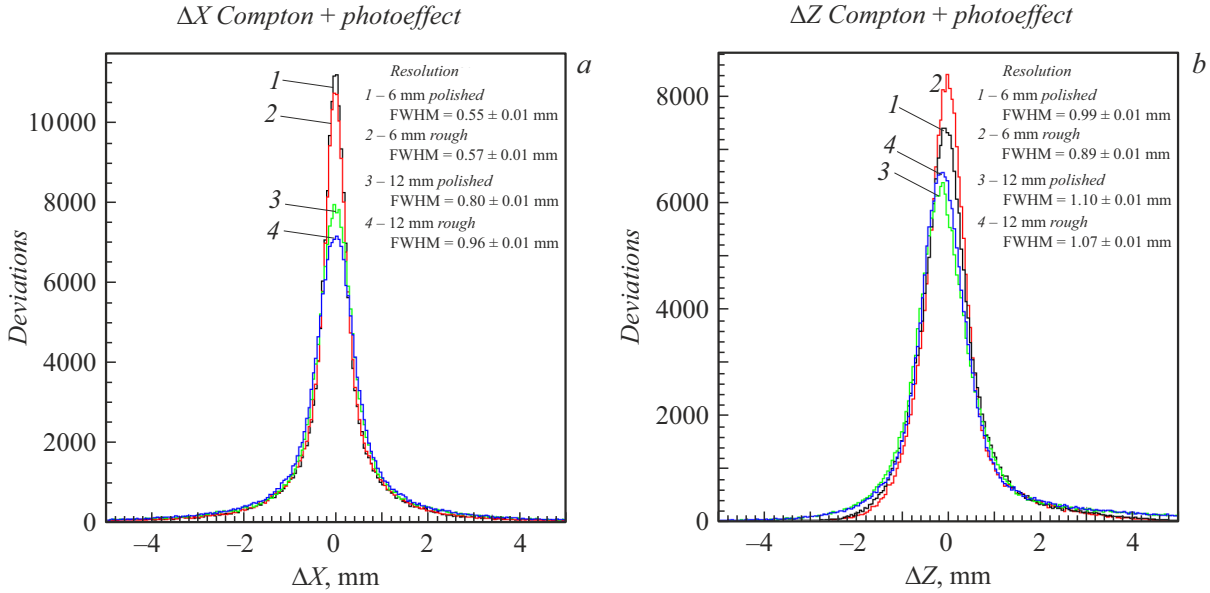

Figure 3. Distributions of deviations of reconstructed coordinates from actual ones ΔX (a) and ΔZ (b) for all detector versions.

photoelectric effect and Compton interactions were used for training (2 000 000 in total), and 200 000 were used to test the network performance. Learning-rate parameter η was decreased linearly every 100 events from $\eta = 0.0005$ to 0.

The results of training of different types of networks are presented in Table 1 ($\Delta R = \sqrt{\Delta X^2 + \Delta Y^2 + \Delta Z^2}$). To calculate the spatial resolution for each combination, the values of deviation of reconstructed coordinates from the actual ones were plotted as histograms with a bin size of 0.01 mm. Since standard functions provided a poor approximation of the shape of the obtained distributions, the resolution was determined by calculating the peak width at half maximum. Thus, the error corresponded to the histogram bin size (0.01 mm). It is worth noting that an increase in the number of layers and neurons in a network does not always lead to better results. This may be attributed to the decaying gradient effect that is observed in large ANNs.

The distribution of the deviation of reconstructed interaction coordinates from the actual ones is shown in Fig. 3. Polished plates provided the best results for coordinates in plane XY, while the distributions obtained for rough plates were the best fit for reconstructing the Z coordinate. In both cases, the distributions for 6-mm-thick plates had higher accuracy than those for 12-mm-thick plates.

Figure 4 shows the distribution of signals from γ-quanta that were absorbed in a region $1 \times 1 \times 1$ mm in size at the

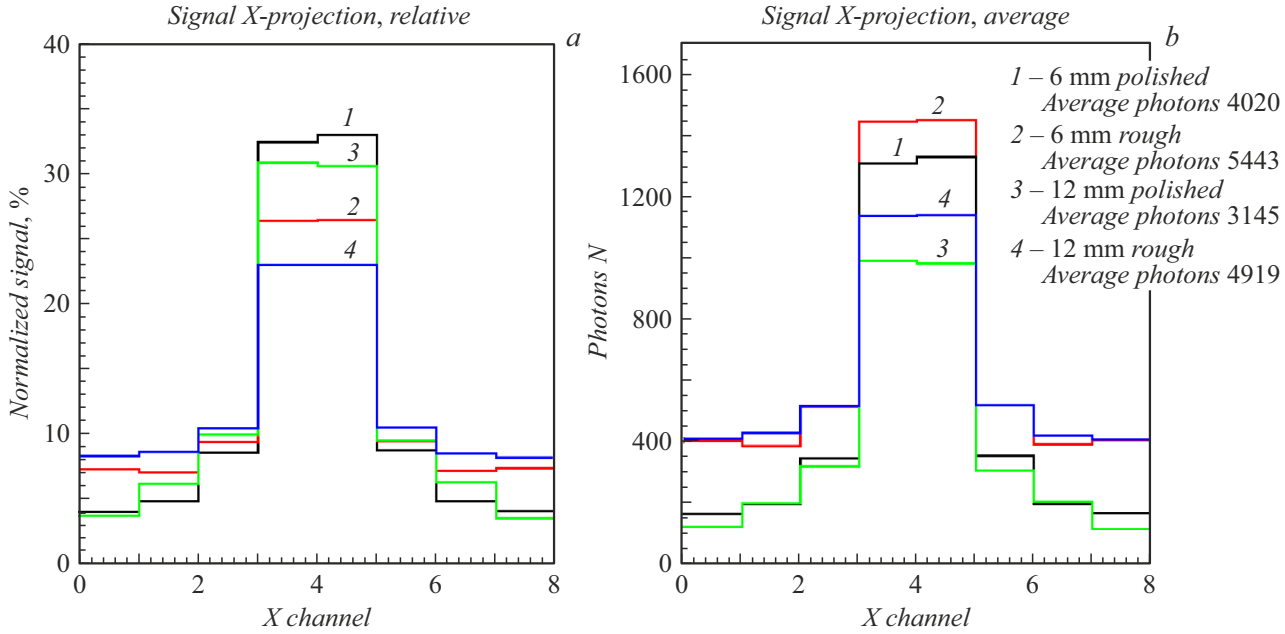

Figure 4. Relative (a) and absolute (b) values of signals corresponding to the photoelectric effect in region $1 \times 1 \times 1$ mm in size at the center of the plate.

Table 2. Efficiencies of absorption of γ-quanta in 12- and 6-mm-thick plates for isotropic and collimated sources

Plate type, source	Efficiency, %	Photoelectric effect, %	Compton effect, %
12 mm, collimated	41.51 ± 0.02	17.42 ± 0.02	23.71 ± 0.02
12 mm, isotropic	45.11 ± 0.02	19.74 ± 0.02	25.36 ± 0.02
6 mm, isotropic	24.08 ± 0.01	12.03 ± 0.01	12.05 ± 0.01

center of the crystal. The distribution shows that the relative fraction of the signal reaching the substrate is smaller in the case of polished plates, but the light loss is greater. Another important factor is that thin plates have a lower γ-quanta absorption efficiency. The efficiencies are listed in Table 2.

A separate comparison of the resolutions obtained in ANN training with isotropic and flat collimated sources was conducted. In both cases, the resolution for a 12-mm-thick rough plate was evaluated. The resolutions for a collimated source obtained with a two-layer ANN with 512 neurons per layer are $\Delta X = 0.99 \pm 0.01$ mm, $\Delta Z = 1.10 \pm 0.01$ mm, and $\Delta R = 1.76 \pm 0.01$ mm. These values are close to the ones given in Table 1. The highest resolution was achieved using a 6-mm-thick rough plate: 0.57 ± 0.01 mm in plane XY and 0.89 ± 0.01 mm along axis Z (along the crystal depth); $\Delta R = 1.19 \pm 0.01$ mm.

The degree of polishing affects significantly the resolution and light collection efficiency of the detector. The distributions obtained with polished plates have a higher resolution in the XY plane, while the distributions for rough plates demonstrate better depth resolution and higher light collection efficiency. In general, thin plates allow one to reach higher spatial resolution levels, but the γ-quanta absorption efficiency is reduced in this case. The neural network reveals the dependence of results on physical properties of the model and may be used as a tool for assessing the resolution of detectors in the course of design work.

Conflict of interest

The authors declare that they have no conflict of interest.

References

[1] L.P. Clemens, J. Peter, Phys. Med., **104**, S98 (2022). DOI: 10.1016/S1120-1797(22)02345-6
[2] M. Freire, S. Echegoyen, A. Gonzalez-Montoro, F. Sanchez, A.J. Gonzalez, Med. Phys., **49** (8), 5616 (2022). DOI: 10.1002/mp.15792
[3] Yu.D. Zavartsev, M.V. Zavertyaev, A.I. Zagumennyi, A.F. Zerrouk, V.A. Kozlov, S.A. Kutovoi, Bull. Lebedev Phys. Inst., **40** (2), 34 (2013). DOI: 10.3103/S1068335613020024].
[4] G. Daniel, M.B. Yahiaoui, C. Comtat, S. Jan, O. Kochebina, J.-M. Martinez, V. Sergeyeva, V. Sharyy, C.-H. Sung, D. Yvon, Eng. Appl. Artif. Intell., **131**, 107876 (2024). DOI: 10.1016/j.engappai.2024.107876

Translated by D.Safin